Inorganic Chemistry

Article

pubs.acs.org/IC

Formation of Nanocrystalline Barium Titanate in Benzyl Alcohol at Room Temperature

Sjoerd A. Veldhuis,[†] Wouter J. C. Vijselaar,[†] Tomasz M. Stawski,[†,‡] and Johan E. ten Elshof*[,†]

[†]Inorganic Materials Science Group, MESA+ Institute for Nanotechnology, University of Twente, P.O. Box 217, 7500 AE Enschede, The Netherlands

[‡]School of Earth and Environment, Cohen Biogeochemistry Laboratory, University of Leeds, Leeds LS2 9JT, United Kingdom

Supporting Information

ABSTRACT: Nanocrystalline barium titanate (8−10 nm crystallite size) was prepared at temperatures of 23−78 °C through reaction of a modified titanium alkoxide precursor in benzyl alcohol with barium hydroxide octahydrate. The room temperature formation of a perovskite phase from solution is associated with the use of benzyl alcohol as solvent medium. The formation mechanism was elucidated by studying the stability and interaction of each precursor with the solvent and with each other using various experimental characterization techniques. Density functional theory (DFT) computational models which agreed well with our experimental data could explain the formation of the solid phase. The stability of the Ti precursor was enhanced by steric hindrance exerted by phenylmethoxy ligands that originated from the benzyl alcohol solvent. Electron microscopy and X-ray diffraction indicated that the crystallite sizes were independent of the reaction temperature. Crystal growth was inhibited by the stabilizing phenylmethoxy groups present on the surface of the crystallites.

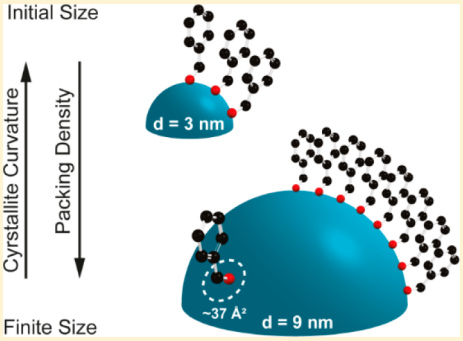

1. INTRODUCTION

Barium titanate (BTO) is used as a high-*k* dielectric material in multilayer ceramic capacitors (MLCC). The industrial trend toward miniaturization leads to ever smaller feature sizes. Commercially used tape casting methods have reached their ultimate limits in terms of downscaling layer thicknesses, so that finer starting powders and compatible off-contact deposition techniques are necessary to enable further miniaturization.

In the last decades, many wet-chemical synthesis routes have been developed to form homogeneous, nanometer-sized BTO particles of high purity.[1−3] Among these methods, sol−gel processing received much attention because of its simplicity, low cost, and control over the composition on a molecular level. However, a disadvantage is that often high postprocessing temperatures are needed to crystallize the amorphous body into the desired BTO perovskite phase, causing phase inhomogeneity and rapid crystallite growth. The alkoxide−hydroxide precipitation method,[4−6] however, is known to form crystalline BTO at temperatures <100 °C, making additional heat treatment unnecessary.[4−8]

Transition metal alkoxides such as Zr and Ti alkoxides are highly reactive toward nucleophilic reagents such as H_2O.[9] Their reactivity can be influenced by one or more factors: (1) steric hindrance by the ligand; (2) the ability to increase the oxidation state of the complex; and (3) the effective charge on the metal. Livage et al. showed the impact of the latter two parameters on gel formation for a range of transition metal alkoxides.[10,11] Gel formation occurs most rapidly for alkoxides with the highest polarizability and the highest tendency to expand their coordination number, i.e. Zr > Ti ≫ Si. Due to their high reactivity, metal alkoxides are often chemically modified by ligand exchange to lower their reactivity and allow easier handling.[9,12−14] It is therefore important to know the effect of chemical modification on the stability of the alkoxide and its susceptibility toward hydrolysis.

Most of these synthesis routes use titanium(IV) isopropoxide in combination with barium hydroxide octahydrate under strongly basic conditions. Unlike for Si alkoxides, the hydrolysis and condensation reactions for transition metal alkoxides (M = Ti or Zr) constitute of a single step reaction in which well-defined poly oxocomplexes are near-instantly formed.[15−18] The amount of water present in the system and the speed of addition are crucial to control the process. An excess of water causes too rapid hydrolysis and may lead to formation of $[Ti(OH)_n]^{(4-n)+}$ species[19] or direct precipitation of amorphous TiO_2,[9] crystallite growth,[8,20] and agglomeration.[7] In order to achieve full control over the hydrolysis−condensation reaction, a good understanding of the underlying chemistry is needed.[9]

In this report we describe the formation of nanocrystalline BTO powder (8−10 nm diameter) at temperatures between 23 and 78 °C. As reported earlier by Stawski et al., a modified Ti alkoxide precursor in benzyl alcohol in the presence of barium hydroxide octahydrate was used in the synthesis.[8,21] Niederberger et al. also showed the importance and active role of

Received: October 1, 2014
Published: November 25, 2014

benzyl alcohol in the nonaqueous synthesis of BTO.[3] However, the two reactions proceed via fundamentally different pathways, i.e. hydrolytic in our case versus nonhydrolytic in the case of Niederberger et al. In our hydrolytic sol–gel synthesis, the reactivity of the $[Ti(OR)_4]$ precursor is reduced by the benzyl alcohol solvent via ligand exchange, without impeding the hydrolysis–condensation reactions at these low temperatures. Essentially, the alkoxide precursor is hydrolyzed by hydrated water that is released from barium hydroxide octahydrate upon mild heating.

To elucidate the formation mechanism, we studied the stability and interaction of both precursors with the solvent and with each other using simplified density functional theory (DFT) calculations, and compared the results with our experimental data.

2. EXPERIMENTAL SECTION

2.1. Chemicals and Materials. Titanium(IV) isopropoxide ($Ti[(i\text{-}OC_3H_7)]_4$), 99.999%), barium hydroxide octahydrate ($Ba(OH)_2{\cdot}8H_2O$, 98.0%), and 2-propanol (99.5%) were purchased from Sigma-Aldrich. Benzyl alcohol (99.0%) was acquired from Acros. All chemicals were used as-received from the suppliers without any further purification. Both titanium(IV) isopropoxide and benzyl alcohol were stored and handled in a water-free environment (<0.1 ppm of H_2O).

2.2. Formation of Crystalline BTO. A stoichiometric amount of barium hydroxide octahydrate was added to a 0.2 mol/dm^3 solution of titanium(IV) isopropoxide in benzyl alcohol. While stirring, the reaction mixture was heated to 35, 45, 60, or 75 °C, whereas one mixture was held at 23 °C (the constant temperature of the lab). After reaction, the as-synthesized powder was centrifuged using a Heraeus Labofuge 300 centrifuge at 8000 rpm for 30 min. The supernatant benzyl alcohol phase was removed by decantation and replaced with 15 mL of 2-propanol. Subsequently, the as-prepared powder was redispersed in 2-propanol and the centrifuging/redispersion steps were repeated. Finally, the dispersion of as-synthesized BTO powder in 2-propanol was poured into a Petri dish and dried at room temperature for 24 h under a constant flow of N_2 to prevent $BaCO_3$ formation.

2.3. Sample Characterization. *2.3.1. X-ray Diffraction (XRD).* Samples synthesized between 23 and 78 °C were characterized with X-ray powder diffraction to confirm the formation of the crystalline $BaTiO_3$ perovskite phase using a Bruker D2 Phaser (Bruker AXS, Delft, The Netherlands) with a LYNXEYE detector. Samples were measured typically from 2θ = 25–90°, with step sizes of 0.02° and 1 s per step. Time-resolved X-ray diffraction was performed to determine the first formation of crystalline phase at temperature between 45 and 150 °C. At intervals of 2–15 min samples were taken from the reaction vessel, and measured using an X'Pert Powder Pro (PANalytical, Almelo, The Netherlands) with a 1D PIXcel detector. Scans from 2θ = 27–35° of the (110) peak were measured with step sizes of 0.026° and 600 s per step. The patterns were further analyzed using the X'Pert Highscore Plus software package (version 3.0e).

2.3.2. Thermogravimetric Analysis and Differential Scanning Calorimetry (TGA/DSC). Weight loss due to dehydration of barium hydroxide octahydrate was measured isothermally using Netzsch STA 449 F3 simultaneous TGA/DSC (Netzsch, Selb, Germany) at 25, 35, 45, 50, 60, and 70 °C. Samples were placed in Pt cups and heated at a constant heating rate of 5 °C/min in technical air (N_2/O_2 = 80/20; flow rate 60 mL/min) to the desired temperature, and held at that temperature for 2–24 h until 7 mol of hydrated water had been released and barium hydroxide monohydrate had formed. All samples were measured at least 3 times in order to determine the experimental error. The weight percentage of benzyl alcohol associated with the presence of a covalently bonded capping layer on the surface of the BTO particles was determined for as-prepared samples, synthesized at 78 °C, and for samples heat-treated at 250 °C for 24 h (bp. benzyl alcohol 205 °C). Samples were placed in Pt cups and heated to 900 °C, using the above-mentioned conditions.

2.3.3. Electron Microscopy Analysis. Samples were investigated by transmission electron microscopy (TEM, 400 keV, FEI Instruments, Eindhoven, The Netherlands) and further analyzed using the ImageJ processing software package (version 1.47q).[22] Crystallite size distributions of selected samples were based on images containing at least 200 different crystallites and recorded at lower magnification.

2.3.4. Small-Angle X-ray Scattering (SAXS). SAXS experiments were performed on the Dutch-Belgium beamline (BM-26B) of the ESRF in Grenoble, France.[23] The samples were irradiated with a X-ray beam energy of 16 keV (λ = 0.0776 nm) and measured using a 2D gas-filled proportional detector (512 × 512 pixels). The recorded scattering vector magnitude was $0.13 < q < 8.2$ nm^{-1}. 1D scattering curves obtained from 2D patterns are plotted as a function of the absolute q-scale with respect to the center of diffraction (i.e., with respect to the beam-stop). The vertical and horizontal q-scale values of the 2D scattering patterns are relative values with respect to the (x,y) = (0,0) *pixel* of the detector. Small quantities of the individual and mixed precursors were measured in sealed glass capillaries (ø = 1.5 mm; glass no. 50; Hilgenberg, Malsfeld, Germany) at different temperatures between 45 and 90 °C.

2.4. Computational Modeling. *2.4.1. Consecutive Ligand Exchange Titanium(IV) iso-propoxide and Benzyl Alcohol.* The model phenylmethoxy ligand ($-OCH_2Ph$) of the benzyl alcohol was created in Spartan'10, and subsequently the equilibrium geometry at ground state was found by energy minimization using a Hartree–Fock 6-31G* basis set. The ligand was taken to be a singly charged anion in singlet state. Subsequently, the ligand was placed at 4 nm from the Ti core of $[Ti(O^iPr)_4]$. In 50 steps, the ligand was moved to the vicinity of the Ti atom (to 1.9 nm distance), and concurrently, the isopropoxide ligand was removed. For every step, the minimum conformation energy was calculated using the energy profile in the ground state, with the semiempirical AM1 method. In the simulation, the oxygen of the phenylmethoxy group binds with the Ti atom of the alkoxide. All simulations were performed in a polarizable benzyl alcohol continuum using the SM8 solvation calculation.[24] Coordination expansion of the monomeric $[Ti(O^iPr)_4]$ species was not taken into account during the simulations, since the electronegative phenyl groups of the benzyl alcohol solvent are thought to effectively shield the Ti-core (see Section 3.2.1).

2.4.2. Electronegativity Changes of the Central Ti-atom. The minimum energy states of all possible ligand exchange complexes (i.e., $[Ti(O^iPr)_4]$, $[Ti(O^iPr)_3(OCH_2Ph)]$, $[Ti(O^iPr)_2(OCH_2Ph)_2]$, $[Ti(O^iPr)(OCH_2Ph)_3]$, and $[Ti(OCH_2Ph)_4]$) in benzyl alcohol were calculated with a Hartree–Fock 6-31G* basis set and the SM8 solvation calculation.[24] The complexes were taken to be charge neutral and in singlet state. A minimum bond length between the phenylmethoxy ligand and the Ti core of 1.95 nm was found.

3. RESULTS AND DISCUSSION

3.1. Dehydration of Barium Hydroxide Octahydrate. The amount of water present in the system during the alkoxide–hydroxide precipitation reaction influences the rate of hydrolysis, and consequently the size and morphology of the powders.[8,20] To control the reaction, the release of water from the Ba precursor was monitored using isothermal thermogravimetric measurements. The weight loss of samples was recorded at constant temperatures below the melting point of $Ba(OH)_2{\cdot}8H_2O$, i.e. 78 °C. Figure 1a shows a typical dehydration curve obtained from a measurement performed at 25 °C. From the start of the measurement, linear weight loss with time was observed until an equivalent mass of 7 mol H_2O water had been released. The time necessary for complete dehydration varied between approximately 1 and 19 h, at isothermal temperatures of 70 and 25 °C, respectively. The phase of the final powder was identified as $Ba(OH)_2{\cdot}H_2O$ using XRD (data not shown), which agreed well with the observed weight loss. The $Ba(OH)_2{\cdot}8H_2O$ phase showed no signs of melting at any temperature.[25]

dx.doi.org/10.1021/ic502410v | Inorg. Chem. 2014, 53, 13188–13196

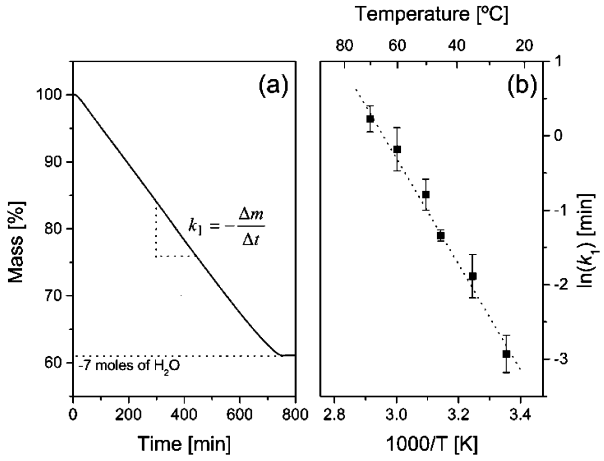

Figure 1. (a) Isothermal dehydration of barium hydroxide octahydrate precursor at 25 °C as measured with TGA/DSC. After dehydration, 7 mol of H_2O were lost and barium hydroxide monohydrate was obtained. The reaction constant k_1 was determined by the slope of weight loss versus time. (b) Arrhenius representation of reaction constant k_1 determined from isothermal measurements at 25, 35, 45, 50, 60, and 70 °C.

The dehydration was governed by evaporation of water and was modeled by a zero-*th* order reaction, as shown in eq 1 to eq 3, where k_1 is the rate constant and t is time.

$$Ba(OH)_2 \cdot 8H_2O \xrightarrow{k_1} Ba(OH)_2 \cdot H_2O + 7H_2O \quad (1)$$

$$\frac{\partial[Ba(OH)_2 \cdot 8H_2O]}{\partial t} = -k_1 \quad (2)$$

$$\frac{[Ba(OH)_2 \cdot 8H_2O]}{[Ba(OH)_2 \cdot H_2O]_0} = -k_1 t \quad (3)$$

Figure 1b shows the exponential behavior of the rate constants obtained from the isothermal TGA measurements. The activation energy for the dehydration of barium hydroxide octahydrate to its monohydrate phase is E_A ~54.7 kJ/mol and was calculated from the slope. Zero-*th* order dehydration kinetics has also been observed for dehydration of other hydrated materials.[26−28] The thermogravimetric experiments show that sufficient water can be released at 25 °C to initiate the hydrolysis reaction of the titanium alkoxide precursor.

3.2. Stability of Titanium(IV) Isopropoxide in Benzyl Alcohol. *3.2.1. Ligand Exchange.* The hydrolytic stability of the highly reactive Ti alkoxide was enhanced by ligand exchange of the phenylmethoxy ligands from the parent solvent, that the precursor solution could be handled under ambient conditions.[8] Similar to hydrolysis−condensation reactions, the consecutive ligand exchanges are thought to follow a series of S_N2 reaction steps,[9,10] resulting in the overall reaction:

$$[Ti(O^iPr)_4] + n\text{ROH} \rightleftarrows [Ti(O^iPr)_{4-n}(OR)_n] + n\text{PrOH} \quad (4)$$

^{1}H NMR measurements (Bruker AV 600 MHz, Wormer, The Netherlands) were performed on solutions of $[Ti(O^iPr)_4]$ in benzyl alcohol to characterize the ligand exchange process. The ligand exchange can be followed by the change in chemical shift of the characteristic septet (−CH) of the isopropoxide ligand (bound to Ti) and isopropanol (exchanged ligand) from approximately δ_H = 4.4 ppm to δ_H = 3.9 ppm, respectively (Figure 2). At room temperature both septets were present, indicating partial ligand exchange and formation of $[Ti(O^iPr)$-$(OCH_2Ph)_3]$, which is in accordance with the findings of Stawski et al.[8] After heating the mixture to 100 °C, only the septet of isopropanol at δ_H = 3.9 ppm was present, showing that full ligand exchange had taken place. These results were compared with the analogous ligand exchange process using acetate ligands. Acetate ligands are frequently used as bidentate ligands to stabilize metal alkoxide precursors.[10,12,13] Figure 2c shows that at RT all ligands are already exchanged. The

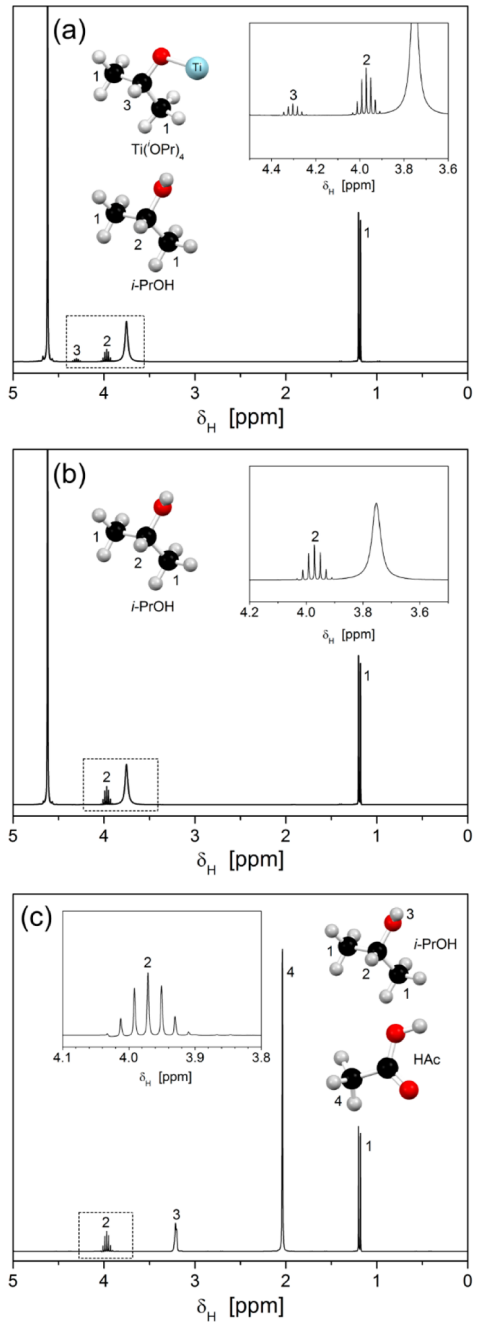

Figure 2. ^{1}H NMR spectra of (a) partially stabilized $[Ti(O^iPr)_4]$ precursor in benzyl alcohol at RT; i.e. $[Ti(O^iPr)(OCH_2Ph)_3]$; (b) $[Ti(O^iPr)_4]$ stabilized by complete ligand exchange of the phenylmethoxy ligands; (c) fully stabilized $[Ti(O^iPr)_4]$ precursor with acetate ligands at RT. The measurement resolution is too low to observe an OH-signal of free isopropanol in (a) and (b).

dx.doi.org/10.1021/ic502410v | *Inorg. Chem.* 2014, 53, 13188−13196

bidentate binding of the acetate to the Ti atom and reduced steric hindrance make it energetically favorable to exchange all ligands. Doeuff et al. showed with FTIR that acetic acid acts as a chelating and bridging ligand.[13] Due to this unidentate binding behavior of acetic acid, polymeric titanium acetate species were formed, without any −OR groups attached to Ti. Our ^{1}H NMR data agree well with the above-mentioned findings, showing that all −OR groups are present as isopropanol.

To obtain insight into the ligand exchange process at RT, the exchange reactions summarized by eq 4 were simulated by DFT. The transition state energy, the Gibbs free energy of the product relative to the starting composition, the partial charge on the Ti atom, and the chemical structure at equilibrium were calculated in a polarizable benzyl alcohol solvent matrix; see Figure 3 and Table 1 (and Supporting Information; Figure S1 and S2). A clear trend was observed in the ligand exchange processes. For every consecutive exchange, the transition state energy increased (i.e., increased activation energy), probably due to steric hindrance by the negatively charged phenyl groups of the phenylmethoxy ligands. As a result, the free energy change of the system upon exchange of the fourth ligand is not favorable ($\Delta G \sim 0$), and this agrees well with the NMR data, which indicate that only 3 ligands are exchanged at RT.

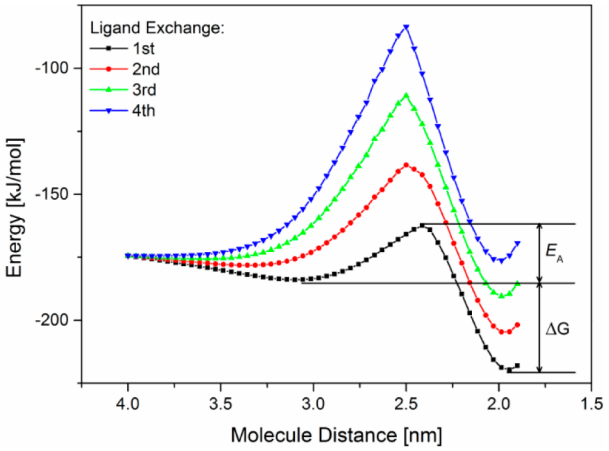

Figure 3. Calculated energy profiles of the four consecutive phenylmethoxy ligand exchanges, and the distance between the approaching benzyl alcohol molecule and the Ti core. For every exchange, the activation energy increases, whereas the Gibbs free energy decreases to almost zero.

Table 1. Energy Data Obtained from the Computational Ligand Exchange Simulations[a]

# Ligand Exchange	Phenylmethoxy ligand		Acetate ligand	
	E_A [kJ/mol]	ΔG [kJ/mol]	E_A [kJ/mol]	ΔG [kJ/mol]
First	21.6	−57.4	26.0	−52.1
Second	39.9	−26.4	33.5	−48.8
Third	64.6	−14.9	36.7	−44.7
Fourth	100.0	−1.9	39.1	−41.5

[a]The activation energy (E_A) and Gibbs free energy (ΔG) are calculated for both phenylmethoxy and acetate ligand exchange reactions.

These results were compared to the same process involving acetate ligands. Although the simulations of the acetate ligand exchange also showed a small increase in activation energy (Table 1), ligand exchange remained favorable at RT for all four exchange reactions ($\Delta G < 0$). This can be explained by the smaller steric hindrance of acetate ligands in comparison to phenylmethoxy ligands, and the results are in good agreement with the data from the ^{1}H NMR measurements.

3.2.2. Partial Charge. The above-mentioned results suggest that the Ti precursor is stabilized against hydrolysis by steric hindrance and the electronegativity of the phenyl groups. However, ligand exchange may also influence the partial charge of the Ti atom and, thus, the intrinsic reactivity of the complex. Several models to calculate the partial charge of a central atom in a complex have been proposed. The simplest model takes only the electronegativity of the direct neighboring atoms into account. The partial charge is then calculated by

$$\delta_{Ti} = V_{Ti} - \left[L_{Ti} + \sum \frac{\chi_{Ti}}{\chi_{Ti} + \chi_O} \cdot B_O \right] \quad (5)$$

Here, δ_{Ti} is the partial charge on the central Ti atom, V_{Ti} the number of valence electrons of Ti, and L_{Ti} the number of lone pair electrons involved. χ_{Ti} and χ_O are the electronegativities of the Ti and O atoms, respectively, and B_O is the number of electrons involved in the bond.

Although the model takes the electronegativity of the direct neighboring oxygen atoms into account, inductive effects of the complete ligand are neglected, as shown in Figure 4a. Livage et al. introduced a more complex model in which the inductive effects of all ligands are taken into account; see Figure 4b.[10,11] The partial charge on the Ti atom is calculated using the average electronegativity of every ligand:

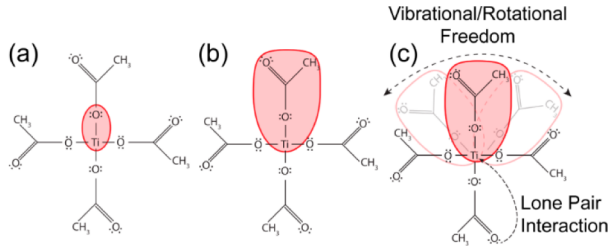

Figure 4. Schematic representation of the partial charge calculation on the central Ti atom of the $[Ti(O^iPr)_4]$ precursor. (a) The electronegativities of only the surrounding oxygen atoms are taken into account; (b) inductive effects of the surrounding ligands are included, as described by Livage et al.;[10,11] (c) proposed model in which inductive effects as well as rotational/vibrational effects of the surrounding ligands are included.

$$\delta_{Ti} = \frac{\bar{\chi} - \chi^0_{Ti}}{k\sqrt{\chi^0_{Ti}}} \quad (6)$$

where $\bar{\chi}$ and χ^0_{Ti} are the mean electronegativity of the ligand and the neutral Ti atom, respectively, and k is Pauling's electronegativity constant (set at $k = 1.36$).[10] Although the second model includes the effect of the complete ligand, the conformation in which these ligands are attached cannot be predicted. Our computational model for ligand exchange was able to include that effect too, and the rotational and vibrational effects of the phenylmethoxy ligand on the positive partial charge could be calculated (Figure 4c). The results of the different models are summarized in Table 2. For the sake of

dx.doi.org/10.1021/ic502410v | Inorg. Chem. 2014, 53, 13188−13196

Table 2. Overview of the Effect of Consecutive Ligand Exchange on the Partial Charge of the Ti Atom[a]

	Electronegativity		Livage		Simulation	
	-OCH_2Ph	-$O(CO)CH_3$	-OCH_2Ph	-$O(CO)CH_3$	-OCH_2Ph	-$O(CO)CH_3$
$[Ti(O^iPr)_4]$	1.81	1.81	0.61	0.61	2.02	2.02
$[Ti(O^iPr)_3(OR)]$	1.81	1.81	0.62	0.65	2.02	1.37
$[Ti(O^iPr)_2(OR)_2]$	1.81	1.81	0.63	0.66	2.03	1.29
$[Ti(O^iPr)(OR)_3]$	1.81	1.81	0.64	0.67	2.04	1.25
$[Ti(OR)_4]$	1.81	1.81	0.64	0.69	2.05	1.19

[a]The results are based on eq 5, eq 6, and our simulations, respectively. Note: the absolute values should not be compared between models; only the trend within a model should be compared.

comparison, the effect of the acetate ligand on the partial charge is also shown. Since the numerical value of the partial charge is calculated differently by each model, only trends within the same model should be compared. Furthermore, the simulations assume the $[Ti(O^iPr)_4]$ precursor to remain monomeric prior to and after ligand exchange,[10,29] in accordance with literature data that suggest that the $[Ti(O^iPr)_4]$ precursor does not form dimeric or oligomeric species, nor does it expand its coordination number, in contrast to $[Ti(OEt)_4]$ and $[Ti(O^nBu)_4]$.[10,29]

As expected, the model described by eq 5 did not predict changes in the partial charge as a result of ligand exchange. The other two models predicted only a slight increase of the partial charge on the Ti atom, implying that the phenylmethoxy ligands do not contribute significantly to an increased stability toward hydrolysis.[16] On the other hand, a clear decrease in partial charge was observed for the acetate ligand, indicating that bidentate binding of the acetate effectively reduces the overall reactivity of the metal alkoxide/acetate. The stability of both the phenylmethoxy and acetate stabilized precursors was further investigated by adding a small amount of water at RT. Whereas the latter solution was stable for days, the phenylmethoxy stabilized solution turned opaque within minutes. These results thus indicate that the Ti precursor is not stabilized by a partial charge decrease of the central Ti atom but rather by the shielding of the phenylmethoxy ligands (i.e., steric hindrance). Figure 5 illustrates the effective encapsulation of

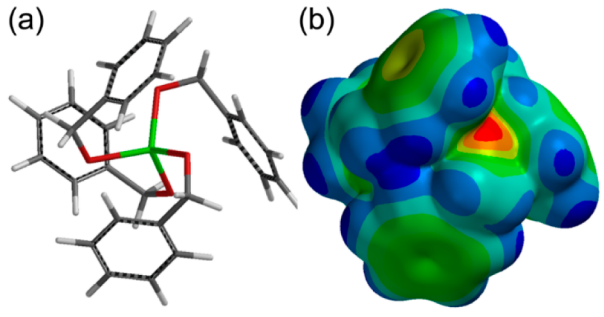

Figure 5. (a) 3D view and (b) electrostatic potential map of the optimized $[Ti(OCH_2Ph)_4]$ structure, i.e. after complete ligand exchange.

the Ti center by ligands for the state with the lowest conformational energy. Concurrently, the low miscibility of water with benzyl alcohol may also have contributed to the lower reactivity of the Ti precursor.

3.3. Interaction between the Ti and Ba Precursors. Small-angle X-ray scattering (SAXS) and diffraction experiments were performed to study the structural evolution of BTO from the observed interactions between the Ti alkoxide and the Ba precursor in benzyl alcohol. Essentially, SAXS probes local electron density fluctuations of a sample by X-ray scattering at very small angles, which makes it possible to extract structural information on length scales up to 500 nm (typically <200 nm).[30,31] The scattered intensity is measured as a function of the modulus of the scattering vector q (nm^{-1}):

$$q = \frac{4\pi}{\lambda} \sin\theta \tag{7}$$

where λ is the wavelength (nm) of the incident beam, and the scattering angle is 2θ. Suspensions of $Ba(OH)_2 \cdot 8H_2O$ in benzyl alcohol were investigated at elevated temperatures to determine the effect of heating on the crystal structure and the release of hydrate water. Figure 6 shows SAXS data of samples heated between 60 and 90 °C. A clear correlation peak is observed at q ~3.9 nm^{-1} for samples heated at 60 °C, which is interpreted as a Bragg peak associated with the Ba−Ba distance in the (101)

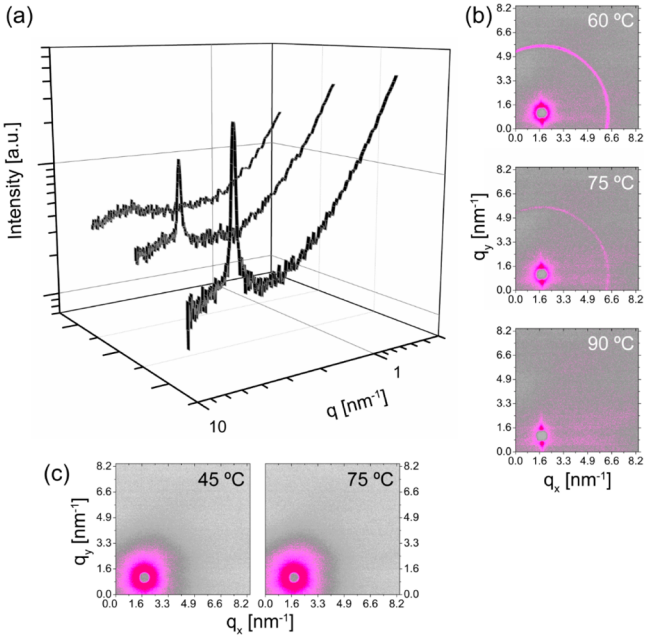

Figure 6. (a) Small angle X-ray diffraction pattern of barium hydroxide octahydrate at different temperatures. Samples measured below the melting point of 78 °C exhibit a diffraction peak at q ~ 3.9 nm^{-1}, correlated to the crystal structure of the Ba precursor. (b) 2D representation of the recorded pattern. (c) 2D small-angle X-ray diffraction pattern of a titanium(IV) isopropoxide and barium hydroxide octahydrate mixture in benzyl alcohol at 45 and 75 °C, respectively. The correlation peak at q ~ 3.9 nm^{-1} disappeared well below the melting point of the Ba precursor; the long-range order in the crystal is lost in the presence of the Ti precursor.

dx.doi.org/10.1021/ic502410v | Inorg. Chem. 2014, 53, 13188−13196

plane of the $Ba(OH)_2{\cdot}8H_2O$ crystal (ICSD # 33741);[32] see Supporting Information Figure S3. In the proximity of its melting point, the diffraction peak was still observed. However, the intensity was lower, suggesting that the processes of decomposition of crystal structure and release of hydrated water were taking place. Above the melting temperature, the characteristic peak at $q \sim 3.9$ nm^{-1} was not visible, indicating that the long-range order of the crystal structure was absent.

The interaction between the Ba and Ti precursors was investigated by addition of titanium(IV) isopropoxide to a $Ba(OH)_2{\cdot}8H_2O$ suspension in benzyl alcohol. Where the Ba precursor in benzyl alcohol clearly showed a Bragg diffraction below 78 °C, no rings were observed in the 2D detector image after $[Ti(O^iPr)_4]$ had been added to the suspension; see Figure 6c. Even at 45 °C, the long-range order of $Ba(OH)_2{\cdot}8H_2O$ was lost in the presence of the Ti alkoxide, showing that even at these low temperatures a strong interaction exists between the two precursors.

The interaction between the precursors, combined with the loss of hydrated water from the $Ba(OH)_2{\cdot}8H_2O$ (as described in section 3.1), thus implies that all reaction conditions for the formation of crystalline BTO are present, even at room temperature.

3.4. RT Formation of Nanocrystalline BTO. *3.4.1. Reaction Pathway.* Syntheses with $Ba(OH)_2{\cdot}8H_2O$ (insoluble) and $[Ti(O^iPr)_4]$ in benzyl alcohol were performed at various temperatures between 23 and 78 °C. Within minutes a white precipitate formed in the solution, indicating that a reaction between the two precursors was taking place. Scanning electron microscopy/energy-dispersive X-ray spectroscopy (SEM/EDX) in combination with XRD confirmed that short reaction times yielded X-ray amorphous TiO_x. Reaction times between 2.5 months and 30 min were necessary for crystalline BTO (Figure 7) to form between 23 and 78 °C, respectively.

The exponential trend in the Arrhenius representation of the inverse crystallization time versus temperature (Figure 7b) shows that the formation of the perovskite phase is driven by the same kinetic processes in the temperature regime of 45–150 °C. The relatively low value of the activation energy, *i.e.* $E_A \sim 65.2$ kJ/mol, implies that the process may be governed by diffusion, possibly by diffusion of Ba^{2+} into the amorphous TiO_x matrix. At temperatures <45 °C, different rate-limiting factors seem to play a role in the crystallization reaction, with an activation energy >200 kJ/mol. Two possible mechanisms have been proposed in the literature for the formation of crystalline BTO, both based on the hydrothermal synthesis route: (1) *in situ* transformation or via (2) dissolution–precipitation.[33] However, based on the experiments presented here, we cannot distinguish between these two mechanisms, and more dedicated time-resolved work should be carried out to elucidate the earliest stages of crystalline BTO phase formation.

3.4.2. Crystallite Formation and Size. The as-synthesized powders were characterized by XRD and TEM; see Figure 8.

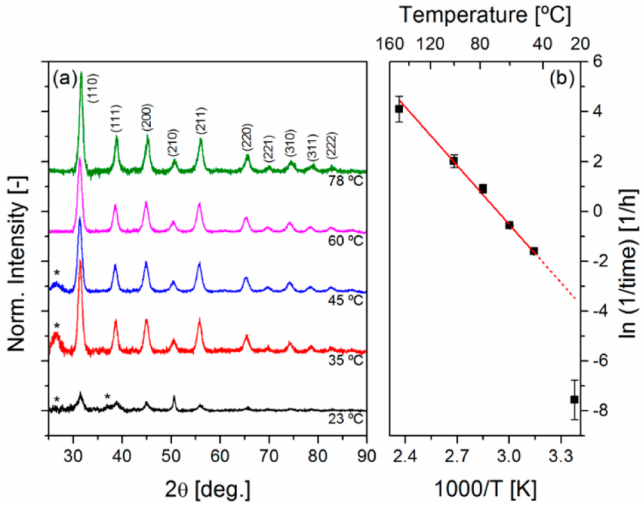

Figure 7. (a) XRD pattern of crystalline BTO powder synthesized at temperatures of 23–78 °C. A minor $BaCO_3$ impurity was present for BTO prepared at temperatures <45 °C. The baseline was subtracted from all patterns and then renormalized to the maximum intensity of the (110) peak at $2\theta \sim 31.4°$ (offset between the patterns: 0.6). (b) Arrhenius representation of the inverse time of the first crystalline phase formation and temperature. A linear trend is observed for temperatures between 45 and 150 °C.

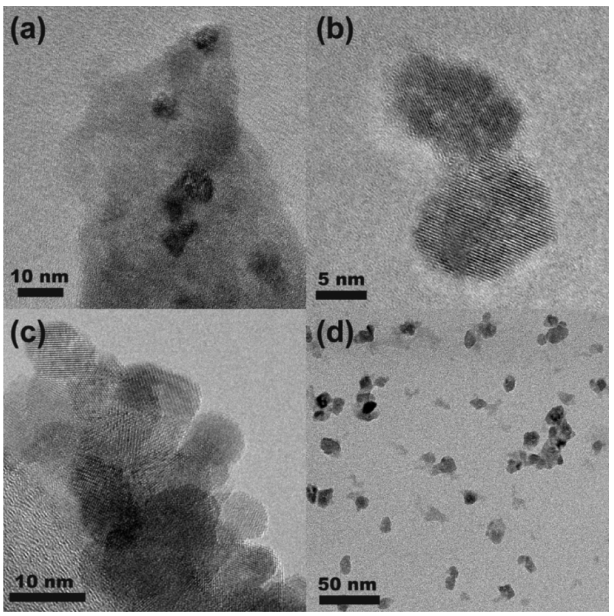

Figure 8. HRTEM images of BTO synthesized at different temperatures. (a) 23 °C, crystalline BTO embedded in an amorphous matrix; (b) 45 °C; (c) 60 °C; and (d) 60 °C. Overview recorded at lower magnification. Sample placed on a Lacey support grid.

Peak broadening analysis of the (111) peak at $2\theta \sim 38.9°$ showed that no significant changes in peak width were observed; that is, no significant crystallite growth occurred, regardless of reaction temperature. The average crystallite sizes were estimated to be approximately 8–10 nm using the Scherrer equation. The sample synthesized at 23 °C, however, showed equally sized crystalline regions embedded in an amorphous matrix (Figure 8a). This might be caused by additional energy barriers dominant in the low reaction temperature regime (Figure 7b), and reaction times longer than 2.5 months are needed to further crystallize the sample at RT. The crystallites formed at temperatures between 35 and 78 °C showed a high degree of crystallinity (Figure 8b–d).

Crystallite size distributions of BTO synthesized at temperatures between 23 and 78 °C revealed that the reaction temperature had no influence on the final crystallite size of the powder. An average final size of approximately 7–9 nm was determined for all samples from TEM images recorded at lower

dx.doi.org/10.1021/ic502410v | Inorg. Chem. 2014, 53, 13188–13196

magnification (see Figure 9). This value is in good agreement with the approximate size calculated from peak broadening in the XRD pattern in the same temperature range.

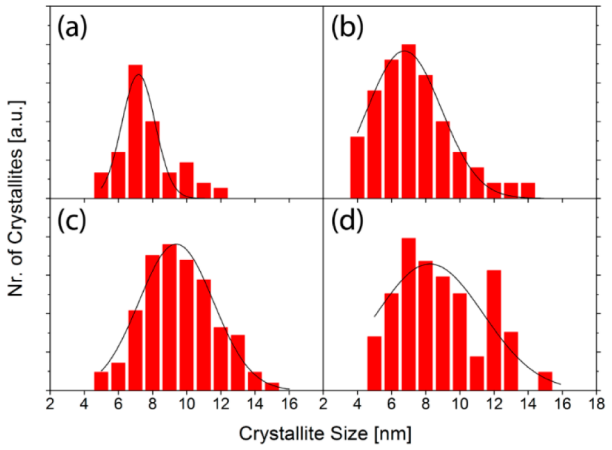

Figure 9. Crystallite size distribution of BTO powder obtained after synthesis at (a) 23 °C, (b) 35 °C, (c) 60 °C, and (d) 150 °C. Crystallite sizes were calculated from at least 200 crystallites from TEM images recorded at lower magnification.

Another series of experiments was carried out to investigate if crystallite growth could be influenced by introducing new precursor material to the reaction mixture. After heating the reactants at 150 °C for 2 h, the mixture containing crystalline BTO was cooled down to RT. Equal amounts of new Ba and Ti precursor material was added, and subsequently the mixture was heated again at 150 °C for 2 h. A single-step synthesis of 4 h at 150 °C was carried out as a control experiment. The BTO powders obtained from both experiments were investigated by XRD and TEM; see Figure 10. Both experiments yielded crystallites of equal size and morphology. Although we showed that the crystallite size increases with increasing amount of water in a previous work,[8] the above-mentioned experiments show that the newly introduced precursor material (i.e., more water present) does not lead to additional crystallite growth but rather to the formation of new nuclei. So the question can be raised why these crystallites all grow to approximately the same size of 7−9 nm, and not larger? Our hypothesis is that benzyl alcohol plays a crucial role in the limited growth of the particles and that it acts as a capping layer on the BTO crystallites' surface (see Figure 11). Niederberger et al. introduced benzyl alcohol as solvent to provide good control over particle shape in the nonaqueous synthesis of BTO, TiO_2, and other metal oxide nanoparticles.[34,35] However, the particle size in their nonaqueous approach is determined mainly by the concentration of Ti precursor.[34]

We hypothesized that since the surface curvature of small crystallites is higher compared to large crystallites, the packing density of benzyl alcohol molecules on the BTO surface is probably lower (Figure 11), and $[Ti(O^iPr)_4]$ can more easily approach the surface hydroxyl groups. As the crystallites grow to their final size of approximately 7−9 nm, the surface curvature is reduced, and the packing of benzyl alcohol molecules on its surface becomes denser. Due to the density of the electronegative phenyl groups on the surface, BTO nanoparticles become effectively shielded from further growth. Cooke et al. showed that benzyl alcohol plays an important role in the formation of TiO_2 nanotubes from carbon nanotubes

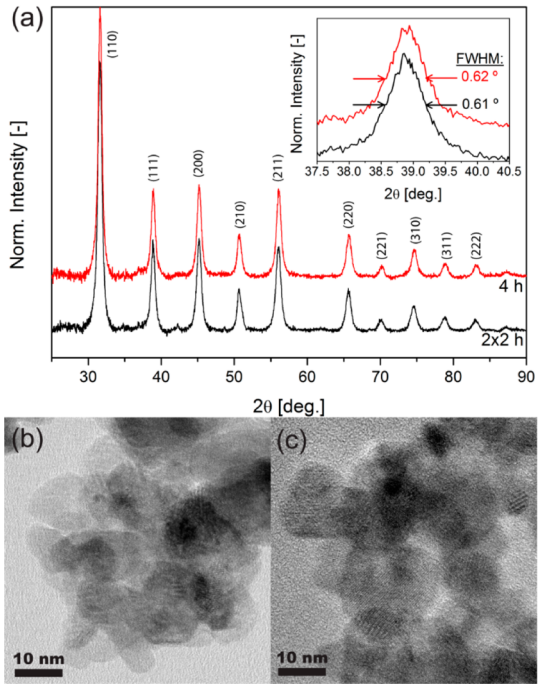

Figure 10. (a) XRD pattern of BTO synthesized for 2 × 2 and 4 h at 150 °C. No differences in fwhm, and thus crystallite size, are observed. (b and c) TEM images of BTO synthesized for 2 × 2 and 4 h at 150 °C, respectively, showing equal crystallite sizes and morphology. Note: the synthesis denoted at 2 × 2 h comprises a regular 2 h synthesis at 150 °C. After cooling the reaction mixture to RT, new precursor material was added and subsequently heated again for 2 h at 150 °C.

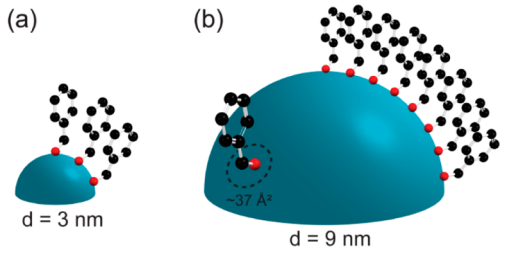

Figure 11. Schematic representation of benzyl alcohol molecules attached to a BTO surface for different particle diameters. (a) 3 nm: high surface curvature−low packing density; (b) 9 nm: low surface curvature−high packing density. The space occupied by one benzyl alcohol on the BTO surface is ~37 Å^2. Effects such as molecule−molecule interactions, molecule rotations, electronegativity of the side groups, stacking, etc. were not taken into account.

(CNTs).[36] The TiO_2 nanotubes were fully covered by benzyl alcohol molecules, preferably parallel to the surface, while the phenyl rings were able to undergo $\pi-\pi$ stacking with the CNTs. If we consider benzyl alcohol molecules as hard spheres covering the BTO crystallites' surface without any interaction with its surroundings, then the surface area occupied by 1 molecule (~37 Å^2) can be estimated from the molecular weight (108.14 g/mol) and density (1.045 g/cm^3) of benzyl alcohol. For nonagglomerated, fully covered BTO crystallites, the surface organic phenylmethoxy monolayer would then contain approximately 5% of the total mass of a BTO crystallite.

Thermogravimetric analysis of BTO powders heat-treated at 250 °C for 24 h, i.e. above the boiling point of 205 °C of benzyl alcohol, and as-prepared samples showed a weight difference of approximately 2.5%; see Figure 12. This value is fairly close to

dx.doi.org/10.1021/ic502410v | Inorg. Chem. 2014, 53, 13188−13196

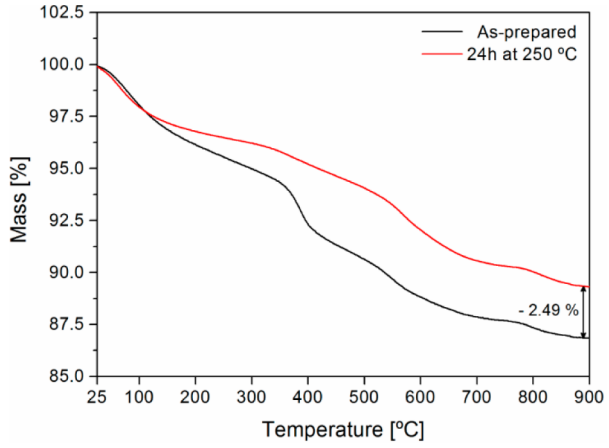

Figure 12. Thermogravimetric analysis of a BTO sample synthesized at 60 °C (red line), and after heat treatment at 250 °C for 24 h (black line). The weight loss of ~7.5% between 400 and 700 °C is probably due to loss of organic moieties such as unreacted alkoxide precursors, and the curing of hydroxyl defects. Since the samples were heated dynamically, mass loss is typically observed at higher temperatures than normal for processes like, e.g., adsorption/chemisorption of water.

the estimated weight loss and indicates that benzyl alcohol may indeed have been present on as-prepared samples.[37] We also observed that the color of as-prepared BTO changed from a slightly yellowish to white upon heat treatment at 250 °C. This also indicates that an organic moiety was initially attached to the surface of the crystallites.

4. CONCLUSIONS

Nanosized crystalline barium titanate powders were successfully synthesized at very low temperatures (23−78 °C) through an alkoxide−hydroxide precipitation reaction of a modified titanium alkoxide precursor in benzyl alcohol and barium hydroxide octahydrate. Our experimental results and simple computational models show that benzyl alcohol plays a crucial role throughout the reaction, from the mixing and modification of the precursor to the formation and growth of the crystalline phase. The phenylmethoxy ligands from the solvent medium stabilized the Ti precursor by steric hindrance, and allowed its subsequent controlled hydrolysis from the hydrated water released by the Ba precursor. The formation of the crystalline phase was dependent on the reaction temperature, and associated with the diffusivity of the Ba^{2+} ions into the amorphous TiO_x matrix. The crystallite sizes, however, were found to be independent of the reaction temperatures. We hypothesized that crystal growth beyond a certain size was hampered by the stabilizing phenylmethoxy groups on the surface of the crystallites.

■ ASSOCIATED CONTENT

Supporting Information

Computational modeling of the phenylmethoxy ligand exchange and the crystal structure of $Ba(OH)_2{\cdot}8H_2O$. This material is available free of charge via the Internet at http://pubs.acs.org.

■ AUTHOR INFORMATION

Corresponding Author

* E-mail: j.e.tenelshof@utwente.nl.

Notes

The authors declare no competing financial interest.

■ ACKNOWLEDGMENTS

This work was financially supported by the Advanced Dutch Energy Materials Program (ADEM).

■ REFERENCES

(1) Phule, P. P.; Risbud, S. H. *J. Mater. Sci.* **1990**, *25*, 1169−1183.
(2) Pithan, C.; Hennings, D.; Waser, R. *Int. J. Appl. Ceram. Technol.* **2005**, *2*, 1−14.
(3) Niederberger, M.; Garnweitner, G.; Pinna, N.; Antonietti, M. *J. Am. Chem. Soc.* **2004**, *126*, 9120−9126.
(4) Viswanath, R. N.; Ramasamy, S. *Nanostruct. Mater.* **1997**, *8*, 155−162.
(5) Yoon, S.; Baik, S.; Kim, M. G.; Shin, N. *J. Am. Ceram. Soc.* **2006**, *89*, 1816−1821.
(6) Frey, M. H.; Payne, D. A. *Chem. Mater.* **1995**, *7*, 123−129.
(7) Flaschen, S. S. *J. Am. Chem. Soc.* **1955**, *77*, 6194.
(8) Stawski, T. M.; Veldhuis, S. A.; Göbel, O. F.; Ten Elshof, J. E.; Blank, D. H. A. *J. Am. Ceram. Soc.* **2010**, *93*, 3443−3448.
(9) Brinker, C. J.; Scherer, G. W. *Sol-gel science: the physics and chemistry of sol-gel processing*; Academic Press, Inc.: San Diego, CA, 1990.
(10) Livage, J.; Henry, M.; Sanchez, C. *Prog. Solid State Chem.* **1988**, *18*, 259−341.
(11) Livage, J.; Sanchez, C. *J. Non-Cryst. Solids* **1992**, *145*, 11−19.
(12) Sanchez, C.; Livage, J.; Henry, M.; Babonneau, F. *J. Non-Cryst. Solids* **1988**, *100*, 65−76.
(13) Doeuff, S.; Henry, M.; Sanchez, C.; Livage, J. *J. Non-Cryst. Solids* **1987**, *89*, 206−216.
(14) Nabavi, M.; Doeuff, S.; Sanchez, C.; Livage, J. *J. Non-Cryst. Solids* **1990**, *121*, 31−34.
(15) Kessler, V. G. *J. Sol-Gel Sci. Technol.* **2009**, *51*, 264−271.
(16) Kessler, V. G.; Spijksma, G. I.; Seisenbaeva, G. A.; Håkansson, S.; Blank, D. H. A.; Bouwmeester, H. J. M. *J. Sol-Gel Sci. Technol.* **2006**, *40*, 163−179.
(17) Schubert, U. *Acc. Chem. Res.* **2007**, *40*, 730−737.
(18) Schubert, U. *J. Mater. Chem.* **2005**, *15*, 3701−3715.
(19) Sugimoto, T.; Zhou, X.; Muramatsu, A. *J. Colloid Interface Sci.* **2002**, *252*, 339−346.
(20) Yoon, S.; Baik, S.; Kim, M. G.; Shin, N.; Kim, I. *J. Am. Ceram. Soc.* **2007**, *90*, 311−314.
(21) Stawski, T. M.; Veldhuis, S. A.; Göbel, O. F.; Podstawka-Proniewicz, E.; Ten Elshof, J. E. *Ceram. Int.* **2012**, *38*, 6911−6917.
(22) Schneider, C. A.; Rasband, W. S.; Eliceiri, K. W. *Nat. Methods* **2012**, *9*, 671−675.
(23) Bras, W.; Dolbnya, I. P.; Detollenaere, D.; Van Tol, R.; Malfois, M.; Greaves, G. N.; Ryan, A. J.; Heeley, E. *J. Appl. Crystallogr.* **2003**, *36*, 791−794.
(24) Marenich, A. V.; Olson, R. M.; Kelly, C. P.; Cramer, C. J.; Truhlar, D. G. *J. Chem. Theory Comput.* **2007**, *3*, 2011−2033.
(25) Lutz, H. D.; Eckers, W.; Christian, H.; Engelen, B. *Thermochim. Acta* **1981**, *44*, 337−343.
(26) Sakata, Y.; Shiraishi, S.; Otsuka, M. *Colloids Surf., B* **2005**, *46*, 135−141.
(27) Koga, N.; Suzuki, Y.; Tatsuoka, T. *J. Phys. Chem. B* **2012**, *116*, 14477−14486.
(28) Perrier, P. R.; Byrn, S. R. *J. Org. Chem.* **1982**, *47*, 4677−4680.
(29) Babonneau, F.; Doeuff, S.; Leaustic, A.; Sanchez, C.; Cartier, C.; Verdaguer, M. *Inorg. Chem.* **1988**, *27*, 3166−3172.
(30) Bras, W. *J. Macromol. Sci.—Phys.* **1998**, *37*, 557−565.
(31) Stribeck, N. *X-Ray Scattering of Soft Matter*; Springer: Berlin Heidelberg, Berlin, 2007.
(32) Sacerdoti, M.; Bertolasi, V.; Ferretti, V.; Accorsi, C. *Z. Kristallogr.* **1990**, *192*, 111−118.
(33) Eckert, J. O., Jr.; Hung-Houston, C. C.; Gersten, B. L.; Lencka, M. M.; Riman, R. E. *J. Am. Ceram. Soc.* **1996**, *79*, 2929−2939.

(34) Niederberger, M.; Bartl, M. H.; Stucky, G. D. *Chem. Mater.* **2002**, *14*, 4364−4370.
(35) Niederberger, M.; Pinna, N.; Polleux, J.; Antonietti, M. *Angew. Chem., Int. Ed.* **2004**, *43*, 2270−2273.
(36) Cooke, D. J.; Eder, D.; Elliott, J. A. *J. Phys. Chem. C* **2010**, *114*, 2462−2470.
(37) Page, K.; Proffen, T.; Niederberger, M.; Seshadri, R. *Chem. Mater.* **2010**, *22*, 4386−4391.